24th International Conference on Renewable Energies and Power Quality (ICREPQ'26)
Santander (Spain), 10th to 12th June 2026
ISBN-13: 978-84-09-82044-3

Stability Control of a SG–PV Integrated Distribution Network Basrah City Case Study

Salam B Abood[1], Ali Jafer Mahdi*[2,3], Ali K Abdulabbas[1]

[1]Electrical Engineering Department, Basrah University, Basrah 61001, Iraq.

[2]Electrical and Electronics Engineering Department, University of Kerbala, Karbala 56001, Iraq.

[3]College of Information Technology Engineering, Al-Zahraa University for Women, Karbala 56001, Iraq, *E-mail: ali.j.mahdi@alzahraa.edu.iq

Abstract. The main challenges facing the Iraqi electrical network are insufficient infrastructure and the fast growth in demand. Advances in renewable energy technologies have made them one of the most actual techniques to address these issues. Because renewable energy systems have a largely static structure and lack significant inertia, they are more susceptible to frequency and voltage fluctuations, which makes the development of advanced control strategies necessary. CYME software was used to model the load demand of a section of Basra's electrical grid, specifically the 5-Mile 33/11 kV substation. Using MATLAB, a hybrid control system combining photovoltaic (PV) generation and a synchronous generator was developed to supply these loads. The system was designed to prioritize local load supply, with any excess power exported to the grid when PV generation increases.

Keywords. PV, Hybrid, RoCoF, CYME, Grid, 5-Mile, MPPT.

1. Introduction

Among of the major challenges facing Iraq's energy sector is the rapidly growing demand for power. Furthermore, it is readily apparent that the system's performance is influenced by its aged infrastructure. The of renewable energy is one of the most effective methods of dealing with these issues because of rapid growth. However, the amount of radiation from the sun has an impact on the electrical power generation from PV systems [1]. As a static device, the system further lacks inertia. To be able to adapt to load variations while keeping high power quality, control systems must be employed to achieve optimum efficiency and manage frequency and voltage fluctuations [2]. By tracking the maximum voltage and current that PV cells can generate in response to variation in temperature and radiation, MPPT technique ensures that PV can create the maximum of power possible [3]. This is achieved by employing a maximum power tracking algorithm from the PV that controls the rate of the DC/DC converter switch. Control systems are implemented for the frequency of operation of the inverter that provides the power to the loads in order to ensure that the voltage and frequency of the power generated by PV are within acceptable limits [4]. Inverters' control systems must be able for imitating conventional generators with the goal to prevent fluctuations in voltage and frequency because they are static devices and lose the moment of inertia [5].

2. Research Aims

For the hybrid system (PV+ Diesel generator) design a maximum power tracking algorithm to ensure the maximum power output from PV and design control system for injecting that power to supply local loads and export excess power to the grid while keeping the voltage and frequency of the generated power within acceptable limits despite changes in loads and solar radiation. Also, building a control system for the power produced from PV so that the supply is allocated to local loads and the surplus is exported to the grid, as shown in Figure. 1. The configuration shown in the Figure. 1 represents a grid-connected PV power system integrated with a dual-grid supply structure and sectionalized load distribution, designed to enhance reliability, operational flexibility, and energy management within a microgrid. After conversion, the AC power is delivered to the bus section (4), which serves as the central distribution node of the system where multiple power sources and loads are interconnected. From the bus section, electrical power is distributed to two different load areas, namely Load Section 1 (5) and Load Section 2 (6). These loads may represent different categories of demand within a facility, such as critical and non-critical loads or separate operational zones within an industrial plant, commercial building, or campus microgrid. The bus section enables controlled distribution of power to these loads while also allowing different power sources to support them depending on operating conditions. In addition to the solar generation source, the system is connected to two independent external utility supplies: Grid1 (3) and Grid2 (9). Grid1 is directly connected to the system upstream of the bus and typically functions as the primary utility supply, supporting the loads whenever the PV generation is insufficient. Grid2, on the other hand, is connected to the bus through Circuit Breaker CB2 (8) and is managed by a tie-line controller (7).

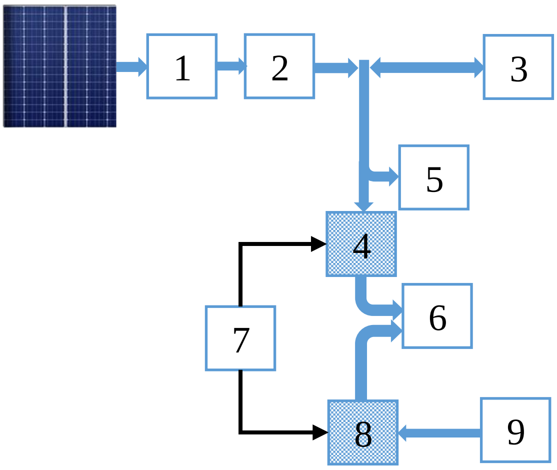

Fig.1. The 5-Mial network distribution with controls of PV

1- The maximum power point tracking (MPPT), 2- Inverter Grid connected, 3-Grid1, 4-Bus Section, 5-Load (Section 1), 6-Load (Section2), 7-Tie-Line Controller, 8- (Circuit Breaker) CB2, 9-Grid2.

The tie-line controller plays a crucial role in coordinating the interaction between the two grids and the internal bus by monitoring voltage, frequency, and phase conditions to ensure safe interconnection. It determines when CB2 should be opened or closed and regulates the flow of power between the system and the secondary grid. Under normal operating conditions, the PV generation and Grid1 jointly supply the loads connected to the bus section. If the PV generation exceeds the load demand, the excess energy can be exported back to Grid1 through the grid-connected inverter, contributing to overall energy efficiency and supporting the external grid. However, if Grid1 experiences disturbances such as voltage drops, outages, or instability, the tie-line controller can activate Grid2 by closing CB2, thereby providing an alternative power path to maintain continuous supply to the loads. In this way, Grid2 acts as a backup or auxiliary source, enhancing the resilience of the system against single-grid failures. Additionally, during periods of high demand, both Grid1 and Grid2 can operate simultaneously, sharing the load and reducing the burden on any single supply source. The tie-line controller ensures that this power sharing occurs in a controlled manner by regulating power exchange across the tie line and preventing reverse power flow or synchronization issues. The presence of the bus section within the topology also allows for effective load management and protection. Furthermore, the configuration supports flexible operating modes such as normal grid-connected operation, renewable priority operation, backup grid operation, and load sharing between multiple sources. Such a topology is commonly used in microgrid systems, industrial power distribution networks, smart grid architectures, and renewable energy integration projects, where maintaining uninterrupted power supply and optimizing the use of renewable generation are key objectives. Overall, this configuration demonstrates a hybrid energy system in which PV power, dual grid connectivity, intelligent control, and sectionalized load management work together to create a reliable, flexible, and efficient electrical power distribution framework.

3. Solar Irradiance Profile and Its Impact on System Stability

Solar Irradiance Profile and Its Impact on System Stability. To ensure realistic operating conditions for the proposed hybrid SG-PV distribution system, actual hourly solar irradiance data recorded at Basrah International Airport during May 2026 were incorporated into the simulation model . The irradiance profile, as shown in Figure. 2, represents the typical daily variation of solar energy availability in southern Iraq and was used as a time-varying input to the PV generation subsystem. Solar irradiance remains negligible during nighttime hours (00:00–05:00 h), resulting in zero PV power production. After sunrise, irradiance increases rapidly from approximately 25 W/m² at 05:00 h to about 620 W/m² at 08:00 h, indicating a steep morning ramp rate. The irradiance continues to rise and reaches values exceeding 880 W/m² between 10:00 h and 14:00 h. The maximum irradiance of approximately 965 W/m² occurs around solar noon (12:00 h), corresponding to the highest available PV output. Following the midday peak, the irradiance gradually decreases from approximately 930 W/m² at 13:00 h to 550 W/m² at 16:00 h, before declining sharply during the late afternoon period. By 18:00 h, the irradiance drops to nearly 150 W/m² and reaches zero at approximately 19:00 h, after which the PV generation ceases completely. From a system stability perspective, these irradiance fluctuations introduce continuous variations in the active power contribution of the PV array. During the high-irradiance interval (10:00–14:00 h), the PV system supplies a substantial portion of the load demand, reducing the power output required from the diesel generators.

4. Basra Distribution Network Description

The distribution network is centered around a 33/11 kV power substation equipped with two transformers, each rated at 31.5 MVA, which supplies operational flexibility and ensures continuity of supply during maintenance or contingency modes. The power substation is fed through two independent 33 kV transmission feeders to improve reliability. The first feeder originates from the Al-Academia 132 /33 kV power substation and has an around length of 9.8 km. The second feeder is supplied from the Sharq Al-Basra 132 /33 kV power substation with a length of appreciate 4.48 km. The dual-feeder configuration enhances the entire dependability of the distribution network, supplies optimal load sharing, and contributes to a rigid stability and efficient operation of the distribution network. Details of the 11 kV outgoing lines that the substation uses to supply the loads are shown in Table I.

5. Network Modeling in CYME

The 5-mile station network simulation was performed using CYME software as shown in Figure. 3, where load flow was performed. the result of load flow is shown in the Table II.

Table I. - The 5-Mile distribution network details

	Feeder ID (11kV)	Length (km)		Load (A)	PF %	Feeder Loading %	NO. Of Tr. 11/0.416 kV (kVA)			Total KVA
		underground	Overhead Line	11kV			250	400	630	
1	SENAA'YAH_5MEIL	0.153	2.175	173	87	58	3	16	0	7150
2	AL-ESKAN	0.236	1.774	203	88	68	5	16	1	8280
3	ALMSHAEL	0.119	0.264	201	89	67	1	14	0	5850
4	4_SHWARAA'	0.215	0.493	213	86	71	5	17	0	8050
5	ALRUDHA_	0.19	0.666	192	87	64	10	10	0	6500
6	ALBALAM	0.137	1.173	202	90	67	0	13	0	5200
7	ALNBRAS	0.171	1.45	183	91	61	6	10	0	5500
8	ALNEDHAL	0.306	0.328	171	89	57	1	15	0	6250
9	AL_QETHARA	0.28	0.717	171	88	57	5	18	0	8450
10	ALHAFEDH	0.189	0.714	235	86	78	1	12	0	5050
11	ALPALADYAH	0.107	0.723	160	89	53	4	20	0	9000
12	ALBEDHAN	0.225	2.967	192	91	64	15	17	0	10550
13	AL JMA'YAH	0.243	0.767	221	87	74	2	20	0	8500
Total		2.571	14.211				58	198	1	94330

Table II. - Load flow of 5-Mile distribution network

	Network ID	Total Load		Total Load		Total Losses		Total Losses	
	33kV	kVA	PF (%)	kW	PF (%)	kVA	PF (%)	kW	PF (%)
A	SHARQALBASRAH_5MIL	24942.60	80.15	19990.67	80.15	106.84	46.50	49.69	46.50
B	ALAKADIMYAH_5MIL	21637.10	80.02	17313.50	80.02	532.62	40.24	214.32	40.24
Total		46579.67		37304.17		639.25		264.01	

6. Dynamic System and Control Modeling in MATLAB/Simulink

A multi-stage control system was designed and built to make the most of the power generated from the solar (PV) cells in supplying the local loads and exporting surplus energy. The descried of these stages as following: (1) The first stage relies on applying the Maximum Power Point Tracking (MPPT) algorithm by controlling the PWM signal of the DC-DC Boost Converter, in order to ensure the PV system operates at the maximum power point under various radiation and temperature conditions [6]: (2) The procedure switches to DC-AC inverter control in the second stage when the solar cell system maximum power output has been reached in the first. In order achieve dynamic system stability and conformity to the electrical grid or related load needs, this stage attempt to control the voltage and frequency at the system output [7]. At that stage, control frequently depends on drop control strategies, which are among the fundamental techniques in low inertia systems, or proportional-integrated controllers (PI-controllers) for voltage and frequency control by using the following equations [8]. Finally, (3) Designing a control system for the power generated by the PV system is the third stage. The loads connected to the station's first section are supplied at the beginning. The second section of the station's loads will be fulfilled if the power generated exceeded the loads; after the local loads have been fully supplied, extra power will be exported to the grid. The flowchart of the control as shown in Figure. 4.

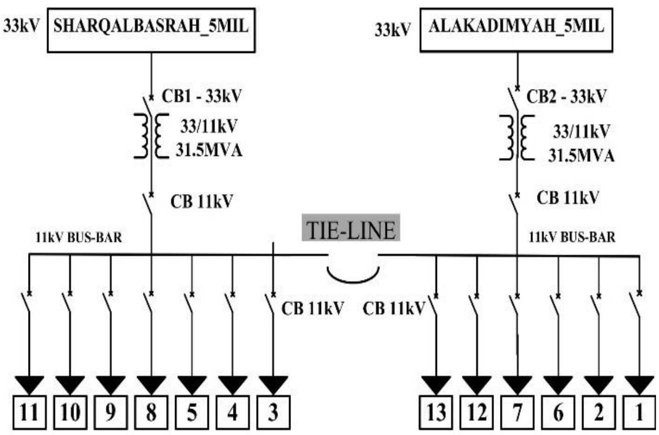

Fig. 3. The 33/11kV Substation of 5-mile proposed network simulated using CYME

$$p = p_0 - k_p\left(f - f_o\right) \quad (1)$$

Where: -

P_o: Reference Effective Power of Inverter.

f_o: Nominal Frequency

f:Measured Network Frequency.

k_p: Droop factor (MW/HZ)

$$Q = Q_0 - k_q\left(V - V_o\right) \quad (2)$$

Where:

Q_o: Reference Reactive Power of Inverter.

V_o: Nominal Voltage .

V:Measured PCC voltage Frequency.

k_q: Droop factor (Mvar/HZ).

$$P_{tie} = P_{G1} + P_{pv} - P_{L1} \quad (3)$$

$$P_{\exp} = P_{pv} - P_{L1} - P_{L2} \quad (4)$$

where:

P_{tie}: Power exchaneg between two section.

P_{L1}: Loacl loads conneced at section one.

P_{L2}: Loacl loads conneced at section two.

P_{G1}: Power supplied from the Grid1.

P_{exp}: Power exported to the grid.

P_{pv} : Power supplied from pv system.

7- Voltage and Frequency Stability

Synthetic droop and virtual inertia are utilized to provide frequency and voltage stability in low-inertia grid-connected PV systems, where the inverter regulates active and reactive output to track the grid voltage and frequency [9].

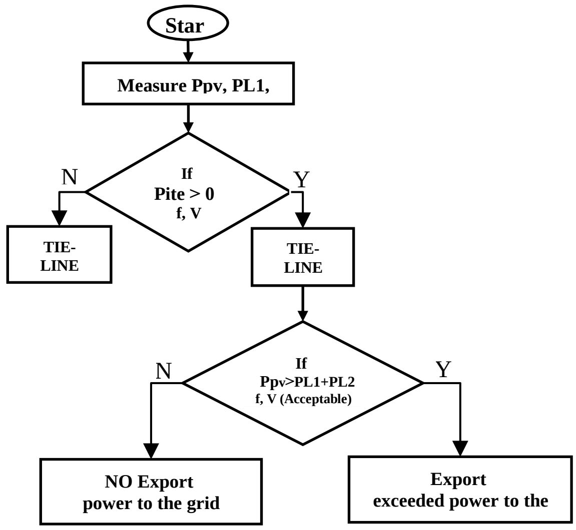

Fig. 4. Flowchart of control to feed the local loads and export electric power

With regard to this, the inverter may effectively improve dynamic stability and the system responding to fluctuations by the following. By increasing frequency stability, lowering rate of change of frequency (RoCoF) through rapid inverter and governor response, preserving voltage through Q and AVR control, and coordinating active and reactive power sharing between sources to ensure steady and effective operation in low-inertia conditions, the controller improves the performance of the mixed diesel–PV system [10]. The important terms are as follows: Frequency stability is to prevent large, successive fluctuations., the controller modifies active power based on frequency variations (P–f droop) and can simulate inertia using the PV inverter [11[,[12]. RoCoF reduction is the rate of frequency change and reducing protection trips, a customized diesel governor and fast inverter action operate together [13],[14]. Voltage regulation is based on the reactive power control (Q droop for PV and AVR for diesel) keeps bus voltages within acceptable limits [15]. Coordination of sources is the droop or control structure makes sure that active and reactive power flow together smoothly, avoiding disputes between diesel and photovoltaic units while optimizing efficiency [16].

8- Simulation Scenarios and Test Cases

The 5-mile network was simulated by MATLAB. A simulation study was conducted for a 5-mile smart electrical distribution network located in Basra city in order to evaluate the integration of photovoltaic (PV) generation into the distribution system. The proposed system includes several control and operational strategies to ensure efficient power generation, voltage regulation, and optimal power management within the network. First, a photovoltaic (PV) power generation system was designed to supply the distribution feeder. To ensure maximum energy extraction from the solar panels under varying solar irradiation conditions, a Maximum Power

Point Tracking (MPPT) technique was implemented. The MPPT algorithm continuously adjusts the operating point of the PV system so that the maximum available power can be generated even when solar radiation levels change. The PV generation unit was connected to the first section of the distribution feeder. Second, a grid-connected inverter control system was designed to regulate the injection of the generated solar power into the distribution network. The inverter control strategy ensures that the output voltage and frequency of the PV system are synchronized with the grid parameters. This synchronization is achieved by controlling the switching pulses of the inverter, allowing stable and efficient power transfer between the PV system and the distribution network. Third, an energy supply priority strategy was implemented to manage the generated solar power within the distribution network. According to this strategy, the locally generated PV power first supplies the local loads connected to the first section of the feeder. When the generated PV power exceeds the demand of the first section, the surplus energy is transferred to supply the loads connected to the second section through a (TIE-LINE) connection between the two sections. During this condition, the power supply from the main utility grid can be disconnected. Furthermore, when the generated PV power becomes sufficient to supply all loads in both sections, the system allows exporting the excess energy back to the main grid. The simulation results obtained from the proposed system operation are illustrated in the figures shown below, demonstrating the dynamic behavior of frequency, voltage, and power under different operating conditions.

For MPPT: - $L_1 = 24.1\text{mH}, C_1 = 258.8\ \mu\text{F}$, $C_2 = 258.8\ \mu\text{F}, R_1 = 20\ \Omega, f_s = 10\text{KHZ}$, $V_{mp} = 38.6\text{V}, I_{mp} = 9.33\text{A}$

For PWM inverter: - $L_2 = 12.67\text{mH}, V_{Grid} = 11\text{kV}$

9- Results and Discussion

After approximately 1.1 s, the oscillations gradually decrease, and the frequency deviation remains within a narrow range of about ±0.01 Hz, indicating that the system successfully reaches steady-state stability. Overall, the maximum observed positive deviation in Area-1 is approximately +0.035 Hz, while the largest negative deviation is around −0.04 Hz, with the system settling in roughly 1.1–1.2 s. The second figure illustrates the frequency deviation behavior in Area-2, where the photovoltaic unit (dfpv), generator-2 (dfG2), and load-2 (dfL2) respond to system disturbances. Compared with Area-1, the deviations in Area-2 are more significant, indicating stronger dynamic effects. First, the voltage stability at Loads 1 & 2 in the 5-mile model was analyzed prior to any PV plant injection. The voltage deviation is shown in Figure. 5.

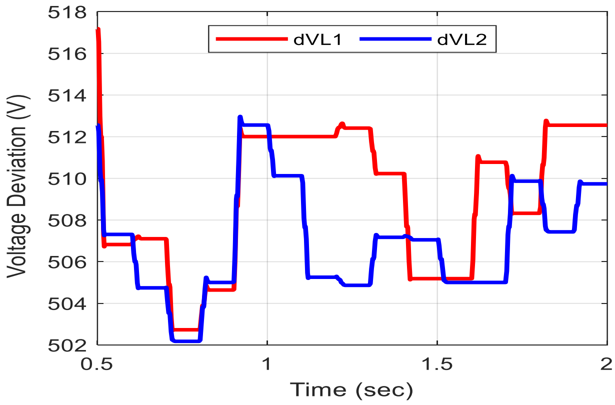

Fig. 5. Voltage deviation at loads 1 and 2 before PV plant injection.

Considering rapid fluctuations in radiation as follows. The irradiance starts at 800 W/m² between 0.2 s and 0.6 s, decreases to 500 W/m² from 0.6 s to 1.2 s, then increases to 600 W/m² from 1.2 s to 1.8 s, and finally rises back to 800 W/m² from 1.8 s to 2.0 s. This profile represents changing sunlight conditions with abrupt transitions in irradiance levels. The control system proceeded to inject the power generated by the PV system, providing local loads priority and exporting extra power to the grid while remaining frequency and voltage within the acceptable limits. as shown in Figures. 6, 7 and 8 below. The first figure presents the frequency deviation responses in Area-1, including the photovoltaic unit (dfpv), generator-1 (dfG1), and load-1 (dfL1). A more pronounced transient event appears near 0.95 s, where the generator response rises to approximately +0.035 Hz, while the load deviation drops to nearly −0.04 Hz, indicating a temporary imbalance between generation and load. Despite this disturbance, the photovoltaic response follows a similar trend to the generator and load, demonstrating effective participation in system support.

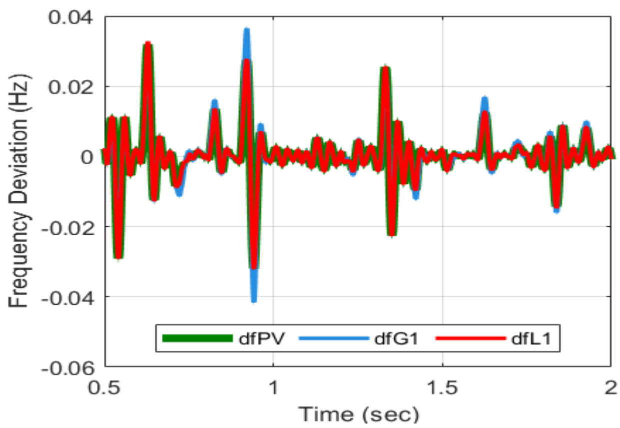

Fig. 6. Frequency response (Area 1).

Shortly after 0.52 s, a severe disturbance produces a large negative frequency deviation of approximately −0.13 Hz in the load signal. The generator deviation at this instant is smaller, reaching about −0.03 Hz, while the photovoltaic unit remains close to zero, suggesting partial mitigation of the disturbance. Around 0.90–0.95 s, the

system exhibits a strong positive oscillation, with the load deviation reaching approximately +0.09 Hz, whereas both the PV and generator responses remain within ±0.03 Hz. Another disturbance occurs near 1.35 s, where the load deviation drops again to nearly −0.08 Hz before gradually damping out. After approximately 1.5 s, all signals converge toward steady conditions with deviations within ±0.01 Hz. In summary, Area-2 experiences larger transient frequency variations, with a maximum positive deviation of about +0.09 Hz and a maximum negative deviation of approximately −0.13 Hz, while the system stabilizes after roughly 1.4–1.5 s.
The first figure illustrates the voltage deviation responses in Area-1 of the smart distribution network operating at a nominal voltage level of 11 kV. The responses correspond to the photovoltaic unit (dVpv), generator-1 (dVG1), and load-1 (dVL1). The results show that all signals follow a similar dynamic pattern with slight differences in magnitude. At approximately 0.5 s, the voltage deviation starts within a range of about 40–60 V, which represents a very small variation compared with the nominal 11,000 V system voltage. Around 0.7 s, a transient disturbance causes a voltage dip where the photovoltaic voltage deviation reaches nearly −30 V, while the generator and load responses decrease to approximately −15 V to −20 V.

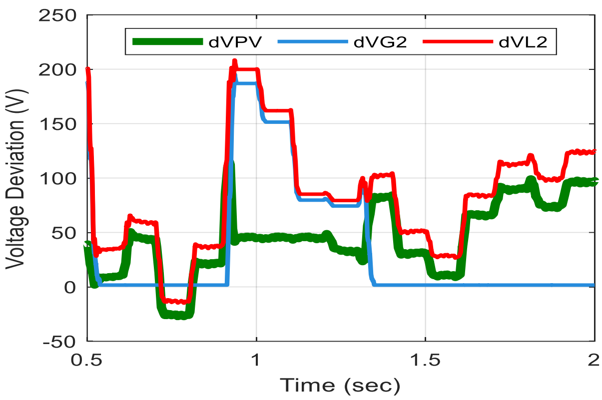

Fig. 7. Voltage response (Area 2).

A significant positive transient appears near 0.9–0.95 s, where the load voltage deviation increases to approximately 120–130 V, the generator response rises to nearly 110–120 V, and the photovoltaic unit reaches about 100–110 V. After this event, the system experiences step-like variations between 40 V and 60 V until around 1.3 s, followed by another increase where the load and generator reach approximately 90–100 V, while the PV unit remains around 80–90 V. Toward the end of the simulation near 1.6–1.7 s, the voltage deviation rises again to about 110–115 V for the load, 100–105 V for the generator, and nearly 90–95 V for the PV unit. Considering the nominal voltage of 11 kV, these variations correspond to deviations of roughly ±0.3% to 1.2%, indicating that the voltage in Area-1 remains well within acceptable operational limits for smart distribution systems. The second figure presents the voltage deviation behavior in Area-2, also operating at the same 11 kV nominal voltage level. The responses include the photovoltaic unit (dVpv), generator-2 (dVG2), and load-2 (dVL2). Compared with Area-1, Area-2 exhibits larger voltage variations, indicating stronger disturbances and higher sensitivity to system events. At the beginning around 0.5 s, the load voltage deviation is relatively high at approximately 200 V, before rapidly decreasing to nearly 30–40 V. Around 0.7 s, a negative dip occurs where the photovoltaic voltage deviation drops to approximately −30 V, while the load decreases to about −10 V to −15 V. A major disturbance occurs near 0.9–1.0 s, where the load voltage deviation sharply increases to approximately 200–210 V, the generator reaches around 180–190 V, and the photovoltaic unit rises to approximately 100–110 V. After this peak, the generator response gradually decreases and eventually approaches 0 V after about 1.4 s, indicating that the generator contribution becomes negligible during the later stage. Meanwhile, the photovoltaic and load voltages continue to vary, reaching approximately 80–100 V near 1.3 s, and increasing again to about 110–120 V toward 1.6–1.7 s. When compared with the 11 kV nominal voltage, these variations correspond to deviations of approximately −0.3% to +1.9%, which remain within the typical permissible voltage limits of smart distribution networks.

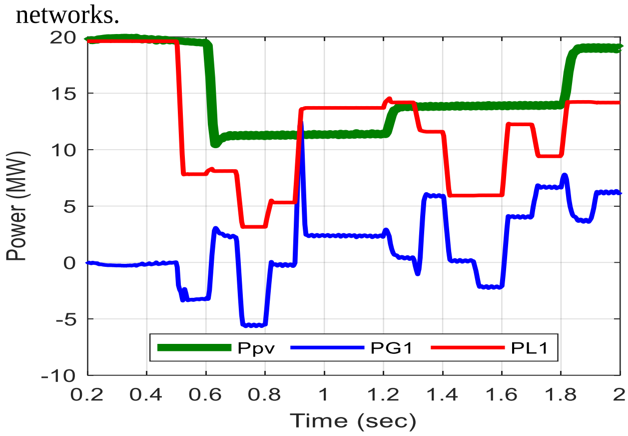

Fig. 8. Power response (Area 1).

10 -Conclusion

The This research investigates an actual distribution network in Basrah city, southern Iraq, where the voltage and frequency stability was analyzed under the integration of a PV power plant. A highly reliable performance was demonstrated in tracking the MPPT under varying solar irradiance conditions, ensuring optimal energy generation. The inverter control strategy effectively regulated the 11 kV network, maintaining frequency deviations within 49.96–50.04 Hz and 49.91–50.14 Hz for Section 1 and Section 2 loads, respectively, while voltage levels were consistently sustained within 10.875–11.025 kV and 10.8–11.025 kV across both sections, reflecting stable operation under dynamic conditions.

Reference

[1] M. Belik, O. Rubanenko, and I. Hunko, "Influence of supplementary installed optical structures on VA characteristics of photovoltaic modules," in Proc. 23rd International Conference on Renewable Energies and Power Quality (ICREPQ'25), Tenerife, Spain, June 25-27, 2025.

[2] R. Fernndez-Vega et al., "Preliminary Characterization of Solar Radiation Patterns in the Canary Islands: An Integrated Approach Combining Clustering and Spatial Interpolation Techniques," in Proc. 23rd International Conference on Renewable Energies and Power Quality (ICREPQ'25), Tenerife, Spain, June 25-27, 2025.

[3] A. Van den Bossche and K. Hafeez, "Excess PV dumping resistor at the DC side of grid tied inverters," in Proc. 23rd International Conference on Renewable Energies and Power Quality (ICREPQ'25), Tenerife, Spain, June 25-27, 2025.

[4] A. Stjepanovic et al., "Development and simulation of an integrated power system based on solar technologies and PEM fuel cells using MATLAB/Simulink software," in Proc. 23rd International Conference on Renewable Energies and Power Quality (ICREPQ'25), Tenerife, Spain, June 25-27, 2025.

[5] R. Dufo-Lopez et al., "Short term energy arbitrage in PV-battery grid-connected systems," in Proc. 23rd International Conference on Renewable Energies and Power Quality (ICREPQ'25), Tenerife, Spain, June 25-27, 2025.

[6] A. Llamazares, S. Martin-Arroyo, A. Bestue Coarasa, and M. Garcia-Gracia, "Stability analysis of an off-grid hybrid power plant for hydrogen production," in Proc. 23rd International Conference on Renewable Energies and Power Quality (ICREPQ'25), Tenerife, Spain, June 25-27, 2025.

[7] M. Khamies, A. H. A. Elkasem, S. Kamel, and M. Hashem, "Optimized frequency stabilization in hybrid renewable power grids with integrated energy storage systems using a modified fuzzy-TID controller," Scientific Reports, vol. 15, Art. no. 20095, Jan. 2025.

[8] P. C. Sahu, "Modelling of an EV based AC microgrid for frequency profile improvement by M-CSA designed Fuzzy-T2-PSS Controller," Progress in Engineering Science, vol. 2, Art. no. 100057, 2025.

[9] S. Somepalli, "Implementing Smart Grid Technology in Developing Countries: Challenges, Opportunities, and Pathways to Sustainable Energy Solutions," Journal of Engineering and Applied Sciences Technology, vol. 6, no. 3, pp. 1-4, 2024.

[10] S. Delgado-Sanchez, J. L. Rodriguez-Amenedo, and S. Arnaltes, "Stability Analysis of Grid-following Converters in Power Systems Depending on Grid Stiffness," in Proc. 23rd International Conference on Renewable Energies and Power Quality (ICREPQ'25), Tenerife, Spain, June 25-27, 2025.

[11] V. Apor and I. Vokony, "The Impact of Renewable Energy on the Stability of Future Power Systems," in Proc. 23rd International Conference on Renewable Energies and Power Quality (ICREPQ'25), Tenerife, Spain, June 25-27, 2025.

[12] M. S. Ibrahim, A. J. Mahdi, and K. A. Al-Anbarri, "Performance Investigation of Wind Turbine Induction Generators connected with a Single-Area Power System," Renewable Energy and Power Quality Journal (RE&PQJ), vol. 20, pp. 403-408, Sept. 2022..

[13] I. Taczi, B. Tozser, and I. Vokony, "Distribution network hosting capacity calculation enhancement through time series analysis and performance index," in Proc. 23rd International Conference on Renewable Energies and Power Quality (ICREPQ'25), Tenerife, Spain, June 25-27, 2025.

[14] J. H. Braslavsky, L. D. Collins, and J. K. Ward, "Voltage stability in a grid-connected inverter with automatic Volt-Watt and Volt-VAR functions," IEEE Transactions on Smart Grid, vol. 10, no. 1, pp. 209-219, Jan. 2019.

[15] D. Arnold, S. Saha, S. T. Ngo, C. Roberts, A. Scaglione, N. Johnson, S. Peisert, and D. Pinney, "Adaptive Control of Distributed Energy Resources for Distribution Grid Voltage Stability," arXiv preprint arXiv:2202.05373, Feb. 2022.

[16] A. Ordono et al., "Adaptive VSG-based grid forming controller for optimal damped response under dynamic grid conditions," in Proc. 23rd International Conference on Renewable Energies and Power Quality (ICREPQ'25), Tenerife, Spain, June 25-27, 2025.